Ma, F., Zhang, X., Hu, J., Li, P., Pan, L., Yu, S., Zhang, Z. (2022): Frequency design of LEO-based navigation augmentation signals for dual-band ionospheric-free ambiguity resolution. - GPS Solutions, 26, 53.

https://doi.org/10.1007/s10291-022-01240-4

Frequency design of LEO-based navigation augmentation signals for dual-band ionospheric-free ambiguity resolution

Fujian Ma[1, 2], Xiaohong Zhang[2, 3*], Jiahuan Hu[2], Pan Li[4], Lin Pan[5], Siqi Yu[6], Zhiyu Zhang[2]

1 Institute of Telecommunication and Navigation Satellites, China Academy of Space Technology, Beijing, China

2 School of Geodesy and Geomatics, Wuhan University, Wuhan, China

3 Collaborative Innovation Center of Geospatial Technology, Wuhan, China

4 German Research Centre for Geosciences GFZ, Potsdam, Germany

5 School of Geosciences and Info-Physics, Central South University, Changsha, China

6 Qianxun Spatial Intelligence Inc., Shanghai, China

Abstract: Due to the spectrum congestion of current navigation signals in the L-band, it is difficult to apply for another two proper frequencies in this band for future low earth orbit (LEO) based navigation augmentation systems. A feasible frequency scheme of using the combined frequencies in the L, S and C bands is proposed. A high-efficiency modulation scheme, termed continuous phase modulation (CPM), is adopted to make full use of the very limited spectrums and satisfy the radio frequency compatibility with the existing navigation systems, radio astronomy, and microwave landing systems. The high propagation loss in the S and C bands is absent for LEO, as the power margin owing to the short-distance propagation has compensated the frequency-dependent attenuation. Besides, for high-precision positioning, we consider the specific integer ratios between frequencies and propose a strategy for LEO precise point positioning (PPP) ambiguity resolution (AR) by directly fixing the L+S or L+C dual-band ionospheric-free (IF) ambiguity. Based on the simulated data, the quality of fractional cycle biases (FCBs) and the performance of PPP AR are analyzed. After

removing the FCBs, 100.0, 99.7 and 71.7% of the fractional parts are within ±0.15 cycles for GPS narrow-lane, LEO L+S dual-band IF and LEO L+C dual-band IF float ambiguities. At user stations, the convergence time of GPS PPP in static mode can be significantly shortened from 17.9 to within 2.5 min with the augmentation of 5.44 LEO satellites. Furthermore, compared with ambiguity-float solutions, the positioning accuracy of GPS AR+LEO AR solutions in east, north and up components is improved from 0.008, 0.008 and 0.027 m to 0.002, 0.003 and 0.011 m for 10-minute sessions, respectively, and the fixing rate after time to first fix is almost 100%.

Keywords LEO-based navigation augmentation; Frequency design; Continuous phase modulation; Ionospheric-free ambiguity resolution; Precise point positioning

Introduction

With the rise of large-scale low earth orbit (LEO) broadband constellations, the navigation augmentation system based on such a platform has become a research focus. Moreover, for China, it is an important part of national comprehensive positioning, navigation and timing (PNT) system and an important development direction of next-generation satellite navigation system (Yang 2016; Xie and Kang 2021). Compared with satellites in medium or high orbits, LEO satellites have the potential to provide stronger navigation signals as they are closer to earth (Lawrence et al. 2017). Also, they travel faster over stations and show rapid changes in spatial geometry. Thus, they can complement the global navigation satellite systems (GNSSs) in terms of availability, robustness, and convergence (Reid et al. 2016; Ge et al. 2018; Wang et al. 2019).

Before the establishment of a LEO-based navigation augmentation system, one of the critical tasks is the frequency design. As a limited and valuable natural resource, frequencies are managed by the International Telecommunication Union (ITU). The signal frequencies of GNSSs and other regional navigation satellite systems are mainly concentrated at the lower L-band from 1164 to 1300 MHz as well as the upper L-band from 1559 to 1610 MHz. Moreover, to mitigate the effect of ionospheric delay, the dual- or multi-frequency signals, of which the central frequencies significantly differ from each other so as to form a low-noise ionospheric-free (IF) combination, are usually employed. Therefore, it is difficult to apply for another two proper frequencies in the L-band as it will further aggravate the congestion and negatively impact the performance of all the existing navigation systems while sharing the same limited resources. To solve this problem, one can either develop very advanced modulation and multiplexing technology to realize compatibility and interoperability or explore signals in new frequency bands (Lu et al. 2015). The ITU also authorizes the radio navigation satellite service (RNSS) to operate in the S-band with a 16.5 MHz bandwidth from 2483.5 to 2500 MHz and the C-band with a 20 MHz bandwidth from 5010 to 5030 MHz. Mateu et al. (2009) and Sun et al. (2017) evaluated the radio frequency compatibility of proposed S-band signals for Galileo and BeiDou, respectively. Irsigler et al. (2004) comprehensively assessed the feasibility of using C-band frequencies for navigation purposes in terms of signal propagation and signal tracking as well as their impacts on satellite payload and receiver design. Some researchers also focused on the modulation schemes of anti-jamming and high-performance navigation signals in these bands (Avila-Rodriguez et al. 2008; Xue et al. 2015).

Although the performance of a single signal in the S or C band cannot surpass that in the L-band because the path losses are higher and the spectrum separation and radio frequency compatibility associated with the limited available bandwidth are worse, a combination of an L-band signal with an S-band or a C-band signal might be an interesting option for navigation since the measurement noises and ionospheric residuals of IF combinations would be smaller. Moreover, the robustness and accuracy of precise point positioning (PPP) could be improved according to Issler et al. (2010). They assumed that if the frequency of an S-band signal was multiple times that of an L-band signal, the wide-lane (WL) ambiguity resolution (AR) using the integer-recovery clock method (Laurichesse et al. 2009) would be eased a lot, as cycle slips could be detected easily, and some intermediate processing step could be simplified.

Unfortunately, no positioning results were provided due to the lack of observations from the designed signals. In fact, thanks to the specific frequency ratio of two signals, the IF ambiguities can even be directly fixed without being decomposed into WL and narrow-lane (NL) ambiguities. Similar concept has been demonstrated in GLONASS IF-based PPP AR since the IF ambiguities already have a wavelength around 5.3 cm owing to the specific frequency ratio of 9/7 between L1 and L2 bands. Banville (2016) calculated undifferenced ambiguities using PPP and formulated double-differenced ambiguities over 12 baselines with a mean inter-station distance of about 850 km for integer cycle resolution. It was found that about 95% of the fractional parts of the estimated double-differenced IF ambiguities agreed well within ±0.15 cycles. In terms of positioning performance, an improvement larger than 20% in east component was observed in static mode for sessions of 2–6 hours. Zhao et al. (2018) also investigated GLONASS PPP with IF AR, but instead of mapping the undifferenced ambiguities to double-differenced ones, the fractional cycle biases (FCBs) were estimated based on the inter-satellite single-differenced ambiguities. The results showed that 89.9, 85.0 and 77.6% of the fractional parts after the removal of FCBs were within ±0.15 cycles for different scales of networks with radii of 500, 1000 and 2000 km, respectively.

Under the premise of compatibility, for the LEO-based navigation augmentation signals, we propose a feasible frequency scheme using the combined frequencies in the L, S and C bands with integer ratios for undifferenced IF AR. The signal propagation characteristics of different bands in LEO are also investigated. In addition, we propose a new undifferenced IF FCB estimation algorithm, and then assess the quality of the FCB estimates as well as the performance of PPP AR based on simulated data.

Frequency design

From the perspective of observation equations, we first explain how it benefits the undifferenced IF AR when two signals are transmitted at two frequencies that are multiple one of the other. Then, the process of frequency selection, as well as the modulation schemes of designed signals, is described. Thereafter, the attenuation in signal propagation for different frequency bands is analyzed.

Benefits to IF PPP AR with specific frequency ratios

For PPP, the dual-frequency IF combination is usually used since the first-order ionospheric delay in the measurements can be eliminated. The corresponding IF pseudorange $P_{r,\mathrm{IF}}^{s}$ and carrier phase $L_{r,\mathrm{IF}}^{s}$ observation equations are given as

$$P_{r,\mathrm{IF}}^{s} = \rho_{r,\mathrm{IF}}^{s} - t^{s} + t_{r} + T_{r}^{s} + b_{\mathrm{IF}}^{s} + b_{r,\mathrm{IF}} + e_{r,\mathrm{IF}}^{s} \quad (1)$$

$$L_{r,\mathrm{IF}}^{s} = \rho_{r,\mathrm{IF}}^{s} - t^{s} + t_{r} + T_{r}^{s} + \lambda_{\mathrm{IF}} N_{r,\mathrm{IF}}^{s} + B_{\mathrm{IF}}^{s} + B_{r,\mathrm{IF}} + \varepsilon_{r,\mathrm{IF}}^{s} \quad (2)$$

where indices s and r refer to the satellite and receiver, respectively, $\rho_{r,\mathrm{IF}}^{s}$ denotes the geometric distance between the satellite and receiver, t^{s} and t_{r} are the clock offsets of the satellite and receiver, T_{r}^{s} is the slant tropospheric delay, λ_{IF} and $N_{r,\mathrm{IF}}^{s}$ are the IF wavelength and ambiguity to be defined, respectively, b_{IF}^{s} and $b_{r,\mathrm{IF}}$ are the IF code hardware delays of the satellite and receiver, B_{IF}^{s} and $B_{r,\mathrm{IF}}$ are the IF satellite-independent and receiver-independent phase delays, respectively, $e_{r,\mathrm{IF}}^{s}$ and $\varepsilon_{r,\mathrm{IF}}^{s}$ are the sum of IF measurement noise and multipath error for the pseudorange and carrier phase observations. All items are in meters except that the $N_{r,\mathrm{IF}}^{s}$ term is in cycles. Other error items such as the phase center offsets and variations, phase windup, relativistic effect and tidal loading are assumed to be precisely corrected with existing models (Kouba 2009).

If the frequency of the second signal is multiple one of the first signal, i.e., $f_2 = kf_1$ with $k \in \mathbf{Z}$, the $\lambda_{\mathrm{IF}} N_{r,\mathrm{IF}}^{s}$ combined term can be formulated as

$$\begin{aligned}\lambda_{\mathrm{IF}} N_{r,\mathrm{IF}}^{s} &= \frac{f_1^2}{f_1^2 - f_2^2}\lambda_1 N_{r,1}^{s} - \frac{f_2^2}{f_1^2 - f_2^2}\lambda_2 N_{r,2}^{s} \\ &= \frac{1}{1-k^2}\lambda_1 N_{r,1}^{s} - \frac{k^2}{1-k^2}\cdot\frac{1}{k}\lambda_1 N_{r,2}^{s} \\ &= \frac{1}{k^2-1}\lambda_1\cdot\left(kN_{r,2}^{s} - N_{r,1}^{s}\right)\end{aligned} \tag{3}$$

where the numeric subscripts denote different carriers and f is the signal frequency. Then, the IF wavelength and ambiguity are defined as

$$\lambda_{\mathrm{IF}} = \frac{1}{k^2-1}\lambda_1 \tag{4}$$

$$N_{r,\mathrm{IF}}^{s} = kN_{r,2}^{s} - N_{r,1}^{s} \tag{5}$$

Specifically, as k, $N_{r,2}^{s}$ and $N_{r,1}^{s}$ are all integers, $N_{r,\mathrm{IF}}^{s}$ has integer property, which shows a promising prospect on IF PPP AR. The corresponding IF wavelength depends on the frequency ratio k and the wavelength of the first signal. According to the frequency allocations of the ITU, we expect k to be 2 between S- and L-band signals, and 4 between C- and L-band signals, respectively.

Frequency selection and signal modulation

Generally, for a single main lobe signal, e.g., a binary phase shift keying (BPSK) modulated signal, the only candidate frequency is the central frequency of the carrier, while for a multi-main lobe signal, e.g., a binary offset carrier (BOC) modulated signal, not only the central frequency but also the frequency points where the main lobes locate are the candidates, as it is possible to track only one of the main lobes with a BPSK-like tracking technique. To make full use of the limited spectrums, the optimal signal allocation should be in the center of the available S and C bands. For S-band frequency design in particular, a central frequency of 2492.028 MHz is suggested to be used considering the interoperability with the Indian regional navigation satellite system (IRNSS). Besides, all candidate frequencies should be multiple times 1.023 MHz, which is a tenth of the GPS fundamental frequency, because all components of the signals are generated by frequency multiplication or division with the same clock. Moreover, the radio frequency compatibility must be considered to avoid harmful interference or spectrum leakage from the designed signals to the existing navigation systems, radio astronomy (RA) and microwave landing systems (MLSs). Therefore, as shown in Fig. 1, for L-, S- and C-band signal designs, central frequencies of 1247.037, 2492.028 and 5020.884 MHz are adopted, respectively. To ensure compatibility with existing navigation signals in the L and S bands, we consider multi-main lobe signals and seek spectral separation. The target frequency couples which satisfy the integer ratios are $f_{\mathrm{L}}+f_{\mathrm{S\text{-}up}}$ and $f_{\mathrm{L\text{-}up}}+f_{\mathrm{C}}$ with f_{L}, $f_{\mathrm{S\text{-}up}}$, $f_{\mathrm{L\text{-}up}}$ and f_{C} of 1247.037, 2494.074, 1255.221 and 5020.884 MHz, respectively.

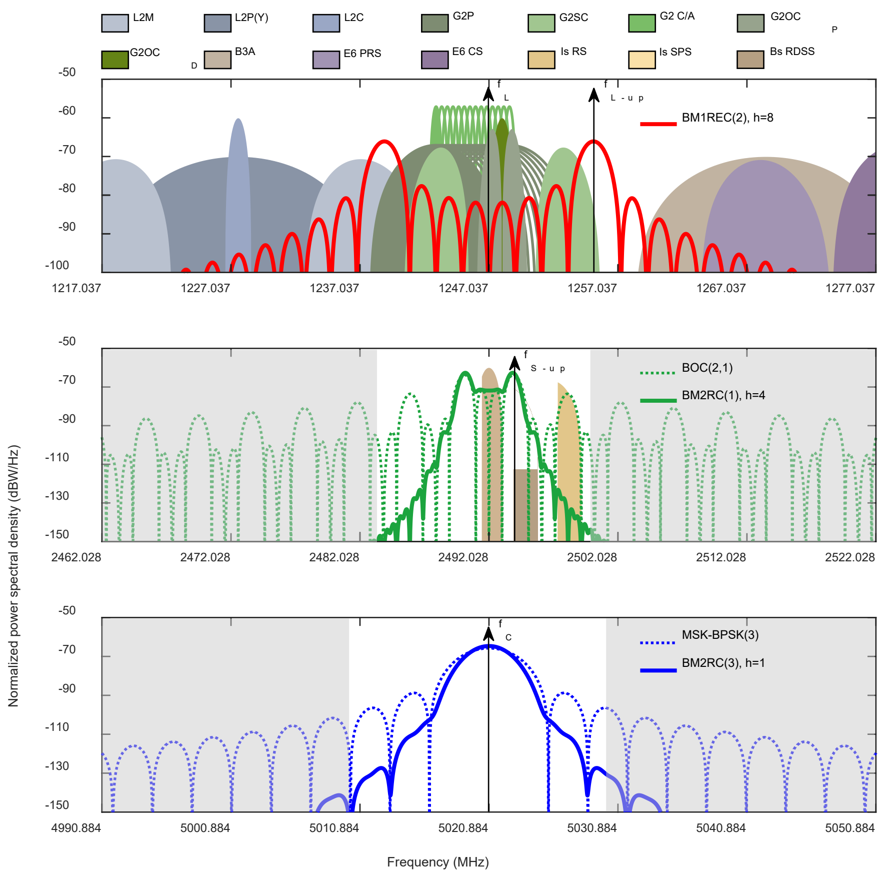

Fig. 1 Normalized power spectral densities (PSDs) of the existing (color-filled) and proposed (solid) navigation signals, as well as the reference (dashed) signals, in the L

(top), S (middle) and C (bottom) bands. The shaded areas are not authorized for RNSS. The black arrows mark the target frequencies

In terms of signal modulation, the early BPSK or the subsequent BOC and multiplexed BOC (MBOC) belong to discontinuous phase modulations resulting in larger spectral side lobes that are not suitable for S- and C-band signal designs with limited spectrum resources and strict out-of-band constraints. In this study, the continuous phase modulation (CPM), which has the characteristics of high spectral efficiency, high power efficiency, continuous phase and constant envelope, is adopted for not only the S- and C-band but also the L-band signal design because a universal modulation scheme can reduce the complexity of a user terminal in multi-band signal processing. The parameter configurations of proposed CPM signals in different bands are given in the Appendix. A longer and smoother frequency pulse is adopted for the S- and C-band signal design to obtain a stronger spectrum roll-off in side lobes. The settings of the symbol duration and modulation index are based on the locations of target frequencies.

To characterize the mutual interference between navigation signals, the spectral separation coefficient (SSC) is calculated as

$$\chi = \int_{-\beta_r/2}^{\beta_r/2} G_{\mathrm{d}}(f) G_{\mathrm{i}}(f) \mathrm{d}f \tag{6}$$

where $G_{\mathrm{d}}(f)$ and $G_{\mathrm{i}}(f)$ are the PSDs of the desired signal and interfering signal, both normalized to the receiver front-end bandwidth β_r. Tables 1 and 2 show the L- and S-band SSCs, respectively. We can see that the proposed BM1REC(2) signal with the modulation index h =8 has satisfactory spectral isolation from different GLONASS signals in the L2 band. Note that although a frequency division multiple access (FDMA) technique is used in the G2P and G2 C/A signals, we only evaluate the typical signals exactly centered at 1246 MHz for simplicity. Regarding the S-band SSCs, both the proposed BM2RC(1) signal with h =4 and the BOC(2,1) reference signal are compatible with the IRNSS S-band restricted service (RS) and standard positioning service (SPS) signals as well as the BeiDou S-band radio determination satellite system (RDSS) signal. However, the side lobes of the proposed signal are notably smaller.

Table 1 SSCs in the L-band, assuming that the receiver bandwidth is 20.460 MHz from 1236.807 to 1257.267 MHz

SSC (dB)		Desired signal					
		G2P	G2SC	G2 C/A	G2OC$_P$	G2OC$_D$	BM1REC(2), h=8
Interfering signal	G2P	-68.40	-73.23	-66.99	-69.59	-69.41	-80.58
	G2SC	-73.23	-68.57	-78.09	-76.17	-81.04	-78.15
	G2 C/A	-66.99	-78.09	-58.80	-79.00	-79.09	-82.08
	G2OC$_P$	-69.59	-76.17	-79.00	-64.60	-67.70	-83.71
	G2OC$_D$	-69.41	-81.04	-79.09	-67.70	-61.77	-82.36
	BM1REC(2), h=8	-80.58	-78.15	-82.08	-83.71	-82.36	-67.60

Table 2 SSCs in the S-band, assuming that the receiver bandwidth is 14.322 MHz from 2484.867 to 2499.189 MHz

SSC (dB)		Desired signal				
		Is RS	Is SPS	Bs RDSS	BOC(2,1)	BM2RC(1), h=4
Interfering signal	Is RS	-67.68	-77.02	-77.25	-75.52	-76.67
	Is SPS	-77.02	-61.73	-66.25	-73.44	-71.12
	Bs RDSS	-77.25	-66.25	-67.39	-69.29	-68.45
	BOC(2,1)	-75.52	-73.44	-69.29	-65.33	-65.12
	BM2RC(1),	-76.67	-71.12	-68.45	-65.12	-64.67

$h=4$

To evaluate the compatibility with the RA band, the power flux density (PFD) of the C-band downlink signal of one satellite is calculated as (Avila-Rodriguez et al. 2008)

$$\mathrm{PFD}_{\mathrm{RA}} = \frac{10^{0.1(\mathrm{EIRP}-L_{\mathrm{A}})}}{4\pi\rho^2} \int_{f\in\Delta f_{\mathrm{RA}}} G(f)\,\mathrm{d}f \tag{7}$$

where EIRP and L_{A} are the equivalent isotropic radiated power (EIRP) and the atmospheric loss, respectively. ρ is the geometric distance in meter, and Δf_{RA} is the RA band from 4990 to 5000 MHz. In this study, a hybrid LEO constellation with an orbital altitude of 1248.171 km, an average number of 5.44 visible satellites and a maximum number of 10 visible satellites is taken for analysis. For details about the constellation configuration, we refer to scheme 4 proposed by Ma et al. (2020). The EIRP of 34.1 dBW is determined based on the link budget in the next section, and the atmospheric loss is set to 0.5 dB. Considering the minimum geometric distance, i.e., the orbital altitude, we obtain the result that the maximum PFDs of the proposed BM2RC(3) signal with $h=1$ and the candidate minimum shift keying (MSK) signal featuring a MSK-BPSK(3) modulation are -199.45 and -146.17 dB(W/m^2), respectively. According to the regulation of the ITU, the maximum PFD must be below the threshold given as

$$\zeta = -171 - X \tag{8}$$

with

$$X = 32 - 25\lg(\psi/2) \tag{9}$$

$$\psi = \arccos(1 - 0.02/N_{\mathrm{sat}}) \tag{10}$$

where N_{sat} is the number of LEO satellites simultaneously radiating into the radio telescope beam, and the intermediate ψ is in degree. In the worst case of 10 visible satellites, the threshold is -196.55 dB(W/m^2), which means only the proposed signal rather than the reference signal is feasible.

To evaluate the compatibility with the MLS band (5030–5150 MHz), the aggregate PFD (APFD) from all visible satellites is calculated as

$$\mathrm{APFD}_{\mathrm{MLS}} = N_{\mathrm{sat}} \frac{10^{0.1(\mathrm{EIRP}-L_{\mathrm{A}})}}{4\pi\rho^2} \int_{f\in\Delta f_{\mathrm{MLS}}} G(f)\,\mathrm{d}f \tag{11}$$

where Δf_{MLS} is any 150 kHz interval within the MLS band. To ensure the MLS compatibility, the APFD shall not exceed -124.50 dB(W/m^2). The maximum APFDs of the proposed and the reference signals are -168.57 and -134.21 dB(W/m^2), and the corresponding integral intervals are both from 5030.00 to 5030.15 MHz. Both signals can satisfy the regulation.

Signal propagation

For satellites in medium or high orbits, high propagation loss is one of the dominant reasons why S- and C-band downlink signals are seldom used for navigation. However, for LEO satellites, the power margin owing to the short-distance propagation may compensate the frequency-dependent attenuation. Fig. 2 illustrates various propagation losses of different signals. The free space loss L_{F} is the main attenuation source, which can be calculated as

$$L_{\mathrm{F}} = \left(4\pi\rho f / c\right)^2 \tag{12}$$

The longer the distance and the higher the frequency are, the higher the free space loss. Besides, as the elevation angle changes, the variation in geometric distance is larger for a LEO satellite than a GPS satellite, thus causing bigger attenuation difference. At 5° elevation angle, the free space losses are 165.6, 171.7, 177.7, and 184.4 dB for the proposed L-band, S-band, C-band, and GPS L1 signals, respectively. In the zenith direction, the corresponding losses are 156.3, 162.3, 168.4, and 182.5 dB.

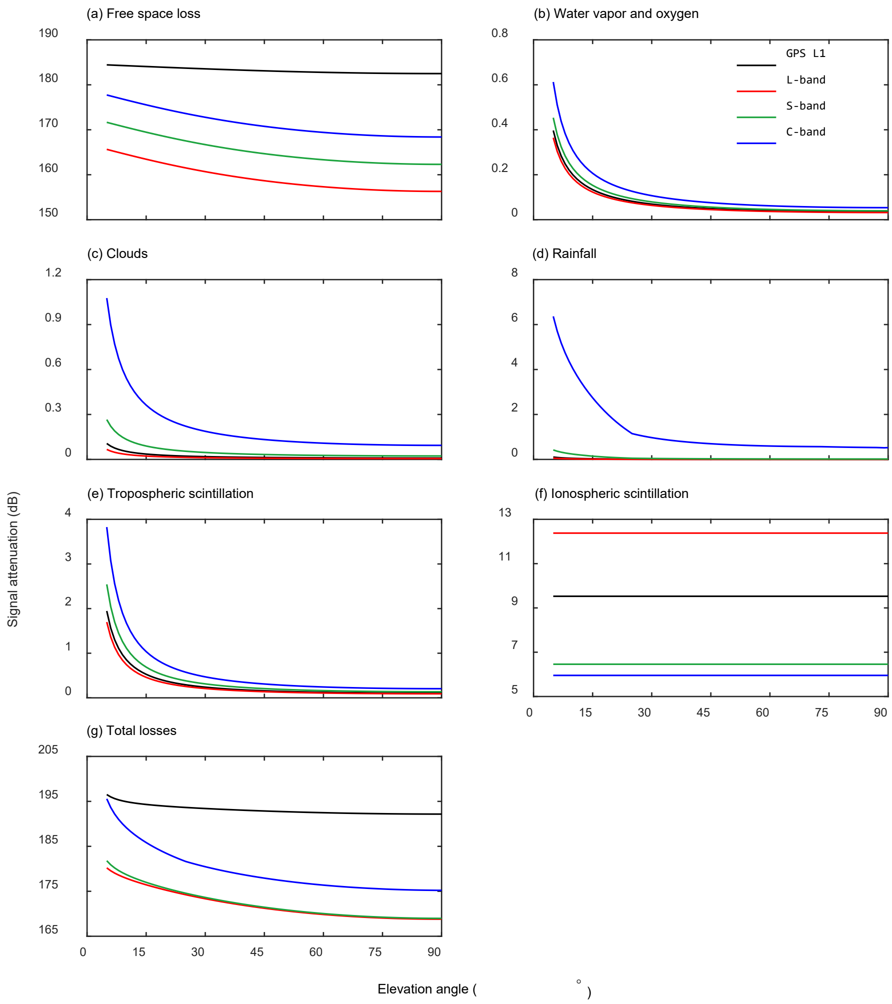

Fig. 2 Propagation losses of the proposed L-, S- and C-band signals transmitted from LEO satellites as well as the GPS L1 signal

Another signal attenuation due to water vapor and oxygen (ITU-R 2013), clouds (ITU-R 2009), rainfall, and tropospheric scintillation (ITU-R 2005, 2015) is calculated using the attenuation models of the ITU. For calculation of the attenuation due to water vapor and oxygen, the standard atmospheric pressure and temperature and a maximum water vapor density of 30 g/m^3 are applied. To calculate the worst cloud attenuation for an exceedance probability of 0.1%, the annual parameter of the total columnar content of cloud liquid water is set to 4 kg/m^2. To calculate the worst rainfall attenuation for an exceedance probability of 0.1%, the input parameters are set as follows: the rain height and the station height above mean sea level are 5 and 0 km, respectively. The latitude of the station is set to 0°. Assuming a tropical thunderstorm happens, a maximum rainfall rate of 145 mm/h is considered. Based on these assumptions, severe rainfall attenuation occurs for the C-band signal at a low elevation angle. The worst attenuation due to tropospheric scintillation for an exceedance probability of 0.1% is calculated by setting the wet term of the radio refractivity to a maximum of 129.

The ionospheric amplitude scintillation is usually characterized by metric S_4 (Van Dierendonck et al. 1993), and the metric at frequency f has a relationship with that at GPS L1 frequency:

$$S_4(f) = S_4(\mathrm{L1})\left(\frac{f_{\mathrm{L1}}}{f}\right)^{1.5} \tag{13}$$

Then, the average intensity attenuation L_{I} can be estimated according to a fitting function (Guo et al. 2019):

$$L_{\mathrm{I}} = -11.57 \times S_4^3(f) + 25.05 \times S_4^2(f) - 7.582 \times S_4(f) + 6.528 \tag{14}$$

Assuming a strong ionospheric scintillation occurs with $S_4(\mathrm{L1}) = 0.7$, the intensity attenuation are 12.4, 6.5, 6.0, and 9.5 dB for the proposed L-band, S-band, C-band, and GPS L1 signals, respectively.

Finally, the total losses of all attenuation sources can be calculated. At 5° elevation angle, the total losses are 180.2, 181.8, 195.6, and 196.5 dB for the proposed L-band, S-band, C-band, and GPS L1 signals. At 90° elevation angle, the corresponding losses are 168.8, 169.0, 175.2, and 192.2 dB. Hence, in the case of similar satellite transmitted power, the received power of all proposed signals will be stronger than that of the GPS L1 signal, particularly for high elevation angle. Overall, the propagation loss will not be an obstacle for the LEO-based navigation augmentation system.

A link budget is also calculated to quantify the impact of the signal upon the power consumption onboard the satellite. As given in Table 3, the required EIRPs are 18.7, 20.3 and 34.1 dBW for proposed L-, S- and C-band signals, respectively.

Table 3 Computation of the required minimum transmitted power for the L-, S- and C-band LEO-based navigation augmentation signals to obtain the same power level on the ground as for GPS L1P(Y) (IS-GPS-200 2010)

Link budget parameter	GPS L1P(Y)	L-band	S-band	C-band
Minimum received power (dBW)	-161.5	-161.5	-161.5	-161.5
Gain of user antenna (dBi)	0	0	0	0
Total losses at 5° elevation angle (dB)	196.5	180.2	181.8	195.6
Required EIRP (dBW)	35.0	18.7	20.3	34.1

Experimental validation

To validate the proposed concept of dual-band IF PPP AR, we first simulate the high-rate GPS+LEO observations as well as the precise orbit and clock products and then generate the FCB products. Unlike the conventional WL and NL FCB estimation method adopted by GPS, a new undifferenced IF FCB estimation algorithm is proposed for LEO.

Data simulation

As shown in Fig. 3, 70 reference network stations and 10 user stations distributed in Europe are selected for FCB estimation and PPP assessment, respectively. Due to the small coverage of a LEO satellite, the reference network stations should be relatively densely and evenly distributed to ensure the reliability of FCB estimates. Receivers at these stations should support simultaneous tracking of GPS dual-frequency $f_{\mathrm{L1}}+f_{\mathrm{L2}}$ and LEO dual-frequency $f_{\mathrm{L}}+f_{\mathrm{S\text{-}up}}$ or $f_{\mathrm{L\text{-}up}}+f_{\mathrm{C}}$ signals. Besides, a LEO satellite passes overhead only in minutes instead of hours, so it is necessary to use high-rate observations to obtain high-precision float ambiguities in preparation for FCB estimation. As shown in Fig. 4, the space segment shows that the 32-satellite GPS constellation and a 100-satellite hybrid orthogonal circular-orbit/Walker LEO constellation (Ma et al. 2020) are selected for analysis.

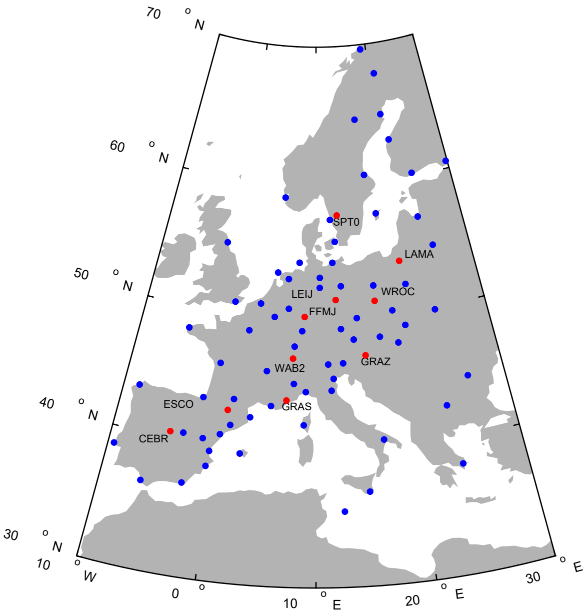

Fig. 3 Distribution of the reference network stations (blue) used for FCB estimation and user stations (red) used for PPP tests

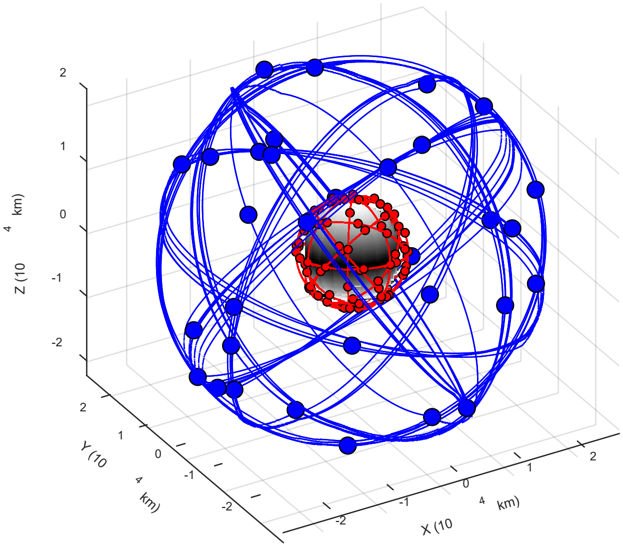

Fig. 4 Trajectories of the GPS (blue) and LEO (red) satellites in the earth-centered inertial frame on March 31, 2019. The dots indicate the initial positions at the midnight epoch

Due to the lack of real observations from LEO satellites to ground stations, we use the simulated observations instead. Besides, to avoid any possible inconsistency in PPP processing, data simulation is also carried out for GPS satellites. For details about the simulation of undifferenced pseudorange and carrier phase observations, we refer to Li et al. (2019). In addition, two issues are worth noting. First, the signal frequencies of the LEO satellites are not the same as those of the GPS satellites. Table 4 gives the wavelengths and error characteristics of different types of observables. We simulate the measurement noises as random noises that obey zero-mean normal distribution with their standard deviations (STDs) dependent on the elevation angles. The higher the elevation angle, the smaller the STD. As the code measurement noise is frequency-independent while the phase measurement noise is basically proportional to the carrier wavelength (Irsigler et al. 2004), neglecting the differences in the signal structure and the carrier-to-noise ratio, the code and phase noises are set to 0.3 m and one-hundredth of the wavelength for a raw observable from the zenith, respectively. The IF wavelength of GPS signals is about 0.6 cm (Dai 2000), and the corresponding IF phase measurement noise is about 6.14 mm, hence it is impossible to distinguish between a noise and an integer cycle, let alone the FCB. However, for proposed L+S scheme, the IF wavelength is about 8.0 cm, and the noise is only about 1.79 mm. For proposed L+C scheme, the IF wavelength is about 1.6 cm, and the noise is only about 0.66 mm. In this case, the IF phase measurement noise is far below the corresponding IF wavelength, which makes it possible to determine the IF ambiguity. In terms of the ionosphere, as the first-order path delay is inversely proportional to the squared signal frequency, the S- and C-band signals will encounter smaller delay than the L-band signal. In terms of the troposphere, unlike the signal attenuation, the path delay is identical for L-, S- and C-band signals as the troposphere is non-dispersive for frequencies below 30 GHz. Second, to omit GPS and LEO precise orbit and clock determination for simplicity, the simulated precise orbit and clock products used for positioning are different from those used to simulate observations by introducing some systematic and random errors to all satellites in all epochs. Whatever the GPS or LEO satellite, the introduced mean 1-dimensional (1D) root mean square error (RMSE) of orbits is 2.1 cm, and the RMSE of clocks is 0.1 ns. Finally, the 1Hz-sampled dual-frequency GPS+LEO observations at all stations on March 31, 2019 and the precise orbit and clock products with 30 s sampling interval are generated.

Table 4 Wavelengths and error characteristics of different types of observables

Type	System	Frequency	Wavelength (cm)	Measurement noise at 90° elevation angle		Scaling factor	
				Code (m)	Phase (mm)	Ionospheric delay	Tropospheric delay
Raw observable	GPS	f_{L1}	19.0	0.30	1.90	1.00	1
		f_{L2}	24.4	0.30	2.44	1.65	1
	LEO	f_{L}	24.0	0.30	2.40	1.60	1

		$f_{\text{L-up}}$	23.9	0.30	2.39	1.58	1
		$f_{\text{S-up}}$	12.0	0.30	1.20	0.40	1
		f_{C}	6.0	0.30	0.60	0.10	1
IF combination	GPS	$f_{\text{L1}} + f_{\text{L2}}$	0.6	0.89	6.14	0	1
	LEO	$f_{\text{L}} + f_{\text{S-up}}$	8.0	0.41	1.79	0	1
		$f_{\text{L-up}} + f_{\text{C}}$	1.6	0.32	0.66	0	1

FCB estimation

Due to the facts that the precise satellite clock products which contain IF code hardware delays following the convention of the International GNSS Service (IGS) are always applied in the data processing, the IF code hardware delay of the receiver is absorbed in the actual receiver clock estimates, and all the code and phase delays are grouped into the ambiguity parameters, (1) and (2) can be rewritten as

$$P_{r,\text{IF}}^{s} = \rho_{r,\text{IF}}^{s} - \overline{t}^{s} + \overline{t}_{r} + T_{r}^{s} + e_{r,\text{IF}}^{s} \tag{15}$$

$$L_{r,\text{IF}}^{s} = \rho_{r,\text{IF}}^{s} - \overline{t}^{s} + \overline{t}_{r} + T_{r}^{s} + \lambda_{\text{IF}} \overline{N}_{r,\text{IF}}^{s} + \varepsilon_{r,\text{IF}}^{s} \tag{16}$$

where $\overline{t}^{s}$, $\overline{t}_{r}$ and $\overline{N}_{r,\text{IF}}^{s}$ are the reparametrized satellite clock, receiver clock and ambiguity as

$$\overline{t}^{s} = t^{s} - b_{\text{IF}}^{s} \tag{17}$$

$$\overline{t}_{r} = t_{r} + b_{r,\text{IF}} \tag{18}$$

$$\overline{N}_{r,\text{IF}}^{s} = N_{r,\text{IF}}^{s} + d_{\text{IF}}^{s} + d_{r,\text{IF}} \tag{19}$$

with

$$d_{\text{IF}}^{s} = \left(B_{\text{IF}}^{s} - b_{\text{IF}}^{s} \right) / \lambda_{\text{IF}} \tag{20}$$

$$d_{r,\mathrm{IF}} = \left(B_{r,\mathrm{IF}} - b_{r,\mathrm{IF}}\right) / \lambda_{\mathrm{IF}} \tag{21}$$

where d_{IF}^{s} and $d_{r,\mathrm{IF}}$ are the IF FCBs of the satellite and receiver, respectively. Affected by them, $\bar{N}_{r,\mathrm{IF}}^{s}$ is estimated as a real-valued constant for a continuous arc if there are no cycle slips in the ambiguity-float PPP solution. To get an ambiguity-fixed solution, the FCBs of high quality must be predetermined and delivered to the users. The more ambiguities can be correctly fixed, the better the performance, therefore both LEO and GPS FCBs are estimated. As the FCB characteristics of LEO may not be consistent with that of GPS due to different orbital altitudes, motion characteristics and signal frequencies, the FCBs of different systems are estimated separately and independently. For GPS, we use the conventional undifferenced WL and NL FCB estimation method (Hu et al. 2019), while for LEO, a new undifferenced IF FCB estimation algorithm is proposed here.

Through transformation, equation (19) can be expressed to

$$\bar{N}_{r,\mathrm{IF}}^{s} - N_{r,\mathrm{IF}}^{s} = d_{\mathrm{IF}}^{s} + d_{r,\mathrm{IF}} \tag{22}$$

Assuming that m satellites are tracked in a network consists of n stations, we have the expression in matrix form as

$$\begin{bmatrix} \bar{N}_{1,\mathrm{IF}}^{1} - N_{1,\mathrm{IF}}^{1} \\ \vdots \\ \bar{N}_{1,\mathrm{IF}}^{m} - N_{1,\mathrm{IF}}^{m} \\ \bar{N}_{2,\mathrm{IF}}^{1} - N_{2,\mathrm{IF}}^{1} \\ \vdots \\ \bar{N}_{2,\mathrm{IF}}^{m} - N_{2,\mathrm{IF}}^{m} \\ \vdots \\ \bar{N}_{n,\mathrm{IF}}^{1} - N_{n,\mathrm{IF}}^{1} \\ \vdots \\ \bar{N}_{n,\mathrm{IF}}^{m} - N_{n,\mathrm{IF}}^{m} \end{bmatrix} = \begin{bmatrix} \mathbf{H}_{11} \\ \vdots \\ \mathbf{H}_{1m} \\ \mathbf{H}_{21} \\ \vdots \\ \mathbf{H}_{2m} \\ \vdots \\ \mathbf{H}_{n1} \\ \vdots \\ \mathbf{H}_{nm} \end{bmatrix} \begin{bmatrix} d_{\mathrm{IF}}^{1} \\ d_{\mathrm{IF}}^{2} \\ \vdots \\ d_{\mathrm{IF}}^{m} \\ d_{1,\mathrm{IF}} \\ d_{2,\mathrm{IF}} \\ \vdots \\ d_{n,\mathrm{IF}} \end{bmatrix} \tag{23}$$

where $\mathbf{H}_{ij}$ is an $(m+n)$-dimensional row vector in which the j-th and $(m+i)$-th elements are 1 while the other elements are 0. Considering the linear dependence of satellite and receiver FCBs, FCB of one satellite is fixed to zero to eliminate the rank deficiency in (23). To acquire accurate and reliable FCBs, the float ambiguity $\bar{N}_{r,\mathrm{IF}}^{s}$ for each continuous arc associated with different propagation paths should be calibrated with strict quality control methods, and $N_{r,\mathrm{IF}}^{s}$ is directly obtained by rounding $\bar{N}_{r,\mathrm{IF}}^{s}$ to the nearest integer. The precision of $\bar{N}_{r,\mathrm{IF}}^{s}$ can be used for determining the weight of an observation. As the initial FCBs of all satellites and receivers are also needed, we first select one satellite tracked by most stations and assume its satellite FCB to be zero, then the rest FCBs can be determined by numerical transfer between common-view stations and satellites. Finally, an iterative least square method is used for precise FCB estimation. In the process of the iteration, the estimated FCBs are applied to correct the undifferenced ambiguities, the corrected ambiguities with fraction parts over a threshold of ±0.25 cycles will not contribute to the FCB estimation in the next iterative step. The FCB results of the last iteration are the initial FCBs of the next iteration. When the FCBs of adjacent iterative results are close enough, the iteration stops, and the satellite FCBs of the final iteration are delivered to users using either the Internet or satellite links.

In the undifferenced FCB estimation mode, the IF receiver hardware delays, i.e., the receiver FCBs, are also estimated. However, it is unnecessary or useless to deliver them to users because the user receivers probably do not participate in the FCB estimation and they have different hardware delays. Even if the hardware configurations are the same, the unknown initial phases are different. To solve this, the inter-satellite single-difference mode can be used while conducting PPP AR.

Results

In this section, we first analyze the quality of the FCB estimates. Then, the ambiguity-fixed solution of LEO constellation-augmented GPS PPP is carried out and evaluated.

Quality of FCB estimates

Fig. 5 shows the FCB estimates and the distribution of a posteriori residuals. During a continuous observation period, the GPS NL FCBs are most stable and vary within 0.02 cycles, followed by LEO L+S dual-band IF FCBs which vary within 0.22 cycles. The LEO L+C dual-band IF FCBs perform worst with the variation even up to 1 cycle.

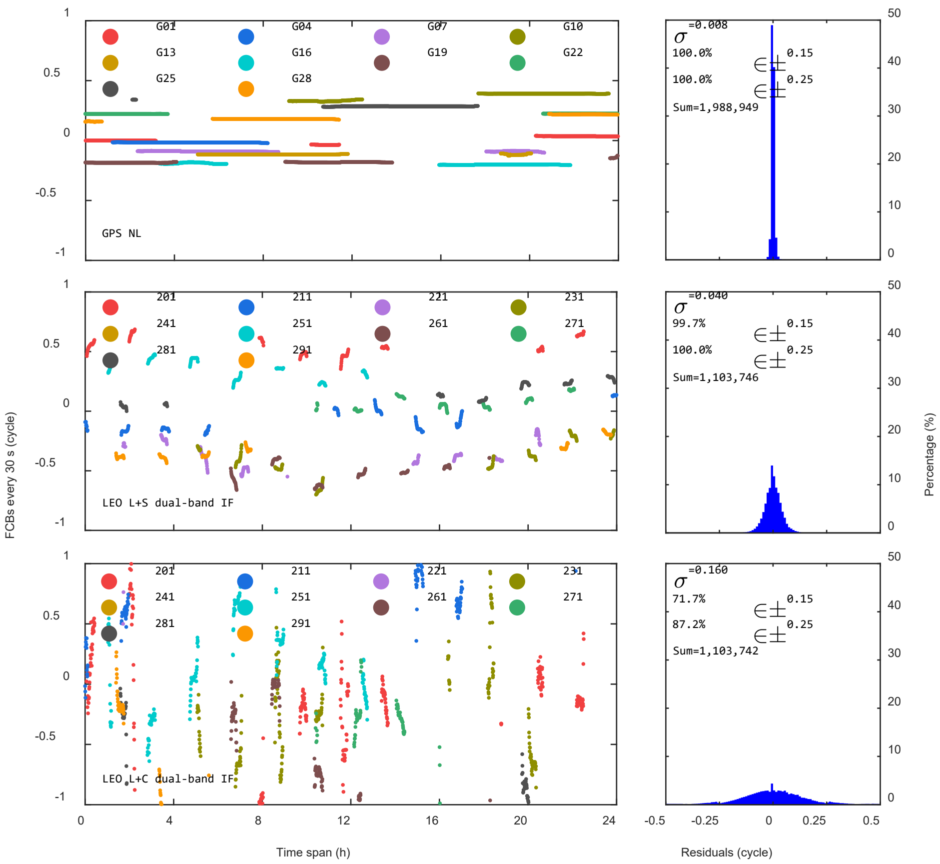

Fig. 5 Time series of GPS NL (top), LEO L+S dual-band IF (middle) and LEO L+C dual-band IF (bottom) FCBs for 10 representative satellites per system estimated every 30 s on March 31, 2019 (left column) and histograms of a posteriori residuals of all 2880 sessions for all satellites (right column). The pseudorandom noise (PRN) numbers of 100 LEO satellites are expressed as three digits and assigned from 201 to 300. σ denotes the STD of the residuals

Then, the quality of the FCB estimates is evaluated by examining the posteriori residuals, which can be regarded as the fractional parts of float ambiguities after the removal of FCBs. For any signal transmission direction, the time from when a satellite signal is generated to when it leaves the antenna is the same, i.e., the hardware delay at the satellite end has nothing to do with the locations of stations. The process of jointly using the observations derived from multiple stations to estimate the FCB of a certain satellite is an unbiased least square estimation, so the residuals are found to approximately obey zero-mean normal distribution, and the closer to zero, the more accurate FCBs we have estimated. For GPS, 100.0% of the NL residuals are within ±0.15 cycles with a STD of 0.008 cycles. Comparatively, the accuracy of LEO L+S dual-band IF FCBs is slightly lower as 99.7% of the residuals are within ±0.15 cycles with a STD of 0.040 cycles. LEO L+C dual-band IF FCBs show the lowest accuracy as only 71.7% of the residuals are within ±0.15 cycles with a STD of 0.160 cycles. The short dual-band IF wavelength, particularly 1.6 cm for the L+C frequency scheme, are easily affected by the unmodeled errors of orbits and clocks, which mainly accounts for the relatively poor temporal stability and accuracy. If the accuracy of FCBs is not high enough, the efficiency of ambiguity search will be reduced and the ambiguities are likely to be fixed incorrectly, which will eventually affect the positioning accuracy, time to first fix (TTFF), and the fixing rate. This impact of inaccurate FCBs on positioning can be reduced to a certain extent through AR preprocessing in which some constraints and accuracy thresholds are set.

PPP AR solution

At user stations, the hourly re-initialized static PPP tests adopting different types of solutions are carried out. In a PPP AR procedure, the inter-satellite single-differenced ambiguities are formed to get rid of the receiver FCBs, and for each system, a satellite with the highest elevation angle is selected as the reference satellite. Corrected with corresponding single-differenced FCBs, the single-differenced GPS WL ambiguities can easily be fixed by rounding averaged the ambiguities over several epochs, while the single-differenced GPS NL and LEO IF ambiguities are resolved with the least-squares ambiguity decorrelation adjustment (LAMBDA) method (Teunissen 1995) and partial ambiguity fixing strategy (Teunissen et al. 1999). Only if at least four ambiguities have been resolved is that epoch considered to be fixable.

Fig. 6 shows the PPP solutions at station ESCO. With the augmentation of LEO satellites with frequency couple $f_{\mathrm{L}} + f_{\mathrm{S\text{-}up}}$, the convergence speed of GPS PPP can be significantly accelerated, especially in east and north components. Moreover, once the ambiguities are correctly fixed to integers, the positioning accuracy is significantly improved and maintained for a long time. Although the GPS+LEO AR solution is not as good as the GPS AR+LEO AR solution due to fewer resolved integer ambiguities, it has successfully verified the feasibility of LEO dual-band IF PPP AR even without the help of GPS PPP AR.

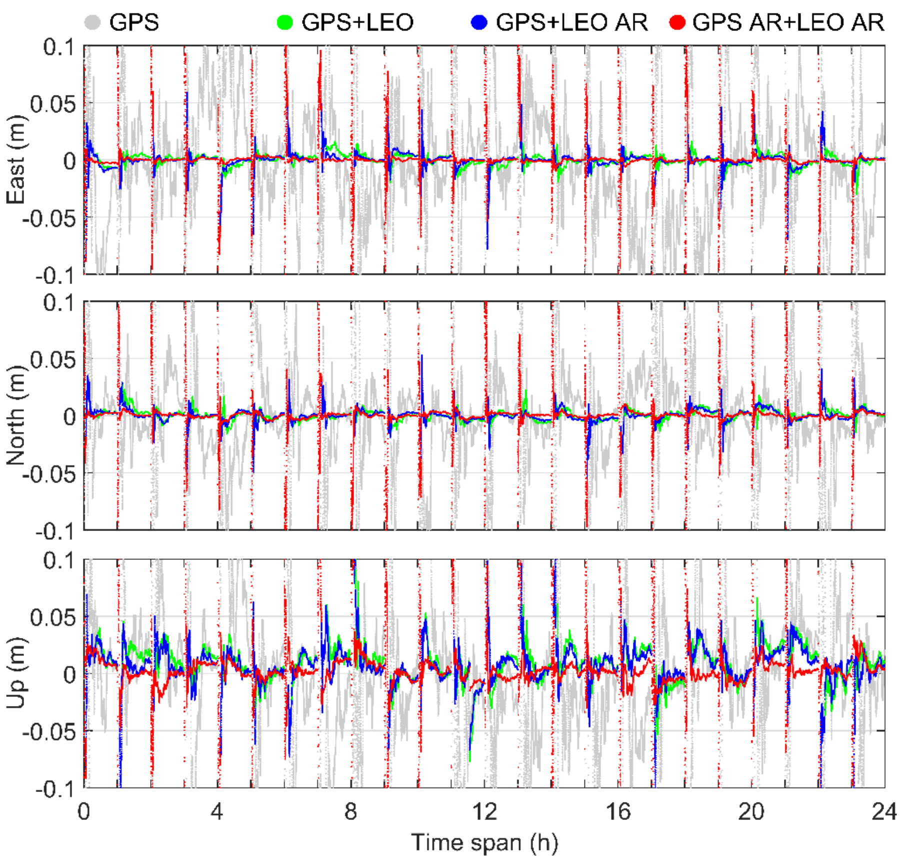

Fig. 6 Hourly static PPP solutions at station ESCO on March 31, 2019. The frequency

couple of LEO satellites is $f_{\mathrm{L}} + f_{\mathrm{S\text{-}up}}$

Fig. 7 shows a close-up of the second session in Fig. 6. To see whether the frequency choice of integer multiple for LEO satellites does impact the positioning, we also repeat the simulation with a non-integer ratio case. As the orange circles shown in Fig. 7, when the frequency choice does not satisfy the integer multiple with one signal frequency slightly different, e.g., replace $f_{\mathrm{L}} + f_{\mathrm{S\text{-}up}}$ with $f_{\mathrm{L}} + f_{\mathrm{S}}$ where $f_{\mathrm{S}} = 2492.028\ \mathrm{MHz}$, the convergence time and positioning accuracy of ambiguity-floated PPP remain unchanged since the IF measurement noises and combination coefficients almost remain unchanged. In fact, what the frequency choice really affects is the AR, only if the frequency choice satisfy the integer multiple could LEO dual-band IF PPP AR be realized according to (3). For the $f_{\mathrm{L}} + f_{\mathrm{S}}$ scheme, even the conventional WL and NL PPP AR could not be realized because the WL wavelength $\lambda_{\mathrm{W}} = (\lambda_1\lambda_2)/|\lambda_2 - \lambda_1|$ is only 24 cm unlike 86 cm for GPS L1+L2. Finally, the positioning accuracy of AR solution for the $f_{\mathrm{L}} + f_{\mathrm{S\text{-}up}}$ scheme after TTFF is found to be significantly better than that of ambiguity-float solution for the $f_{\mathrm{L}} + f_{\mathrm{S}}$ scheme.

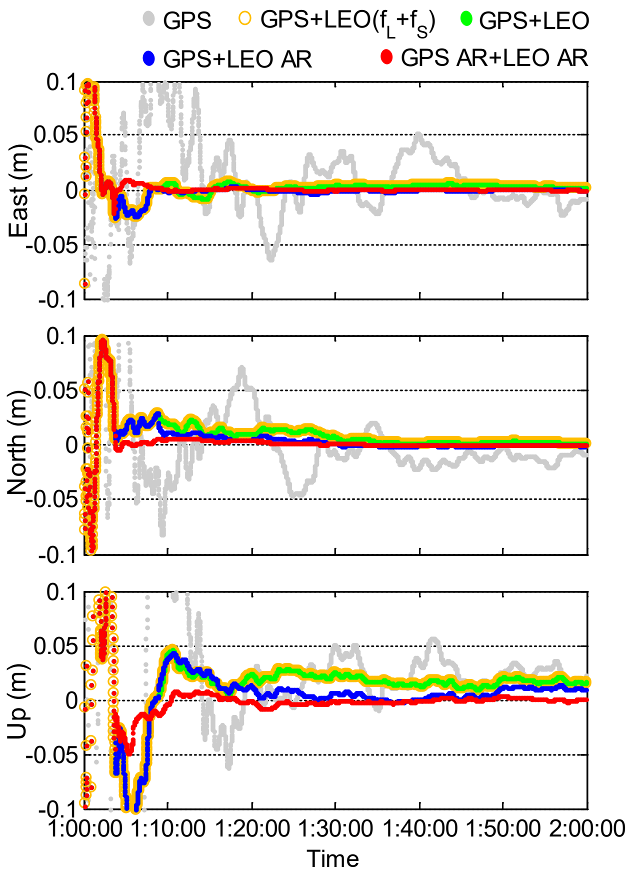

Fig. 7 Static PPP solutions at station ESCO from 1:00:00 to 1:59:59 on March 31, 2019. The frequency couple of LEO satellites is $f_L + f_S$ for the orange scheme, while it is $f_L + f_{S\text{-up}}$ for other schemes

When the frequency couple $f_{L\text{-up}} + f_C$ is adopted by LEO satellites, as shown in Fig. 8, similar results are found except for GPS+LEO AR solution. The green and blue curves are overlapped, which means the IF ambiguities of LEO can barely been resolved. Two reasons may account for this. On one hand, the accuracy of L+C dual-band IF FCBs is not as good as that of L+S ones. On the other hand, due to the short IF wavelength, the accuracy of IF float ambiguity expressed in cycle is too low to be used for AR.

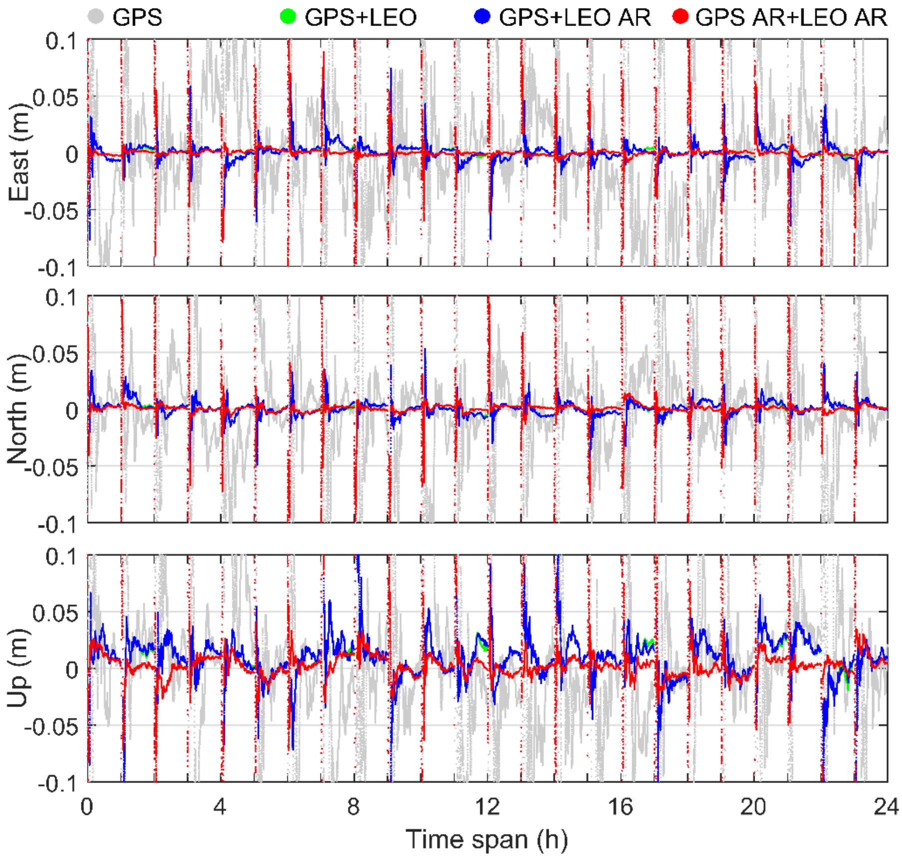

Fig. 8 Hourly static PPP solutions at station ESCO on March 31, 2019. The frequency couple of LEO satellites is $f_{\text{L-up}} + f_{\text{C}}$

Then, the statistical results, including convergence time, TTFF, fixing rate, and positioning accuracy, are given in Table 5. We define the convergence time as the time required to ensure that the positioning errors in both east and north components are less than 0.1 m and maintain for at least 10 min, and the TTFF is defined as the time taken for the ambiguity-fixed solution to be successfully achieved for at least 3 epochs. The fixing rate is defined as the ratio of the number of fixed epochs to the number of total epochs after TTFF. It is found that the convergence time of GPS PPP can be significantly shortened from 17.9 to within 2.5 min with the augmentation of LEO satellites. The convergence time is a bit shorter for the L+C than L+S scheme owing to the smaller measurement noise. The TTFF of GPS AR+LEO AR is about 5.0 min, while it is 9.9 and 55.6 min for GPS+LEO AR adopting the L+S and L+C schemes, respectively. The fixing rate is low for GPS+LEO AR mainly because of the small number of visible LEO satellites. In addition, the AR solution has an advantage in terms of positioning accuracy. Compared with ambiguity-float GPS+LEO PPP, the positioning accuracy within 10 min of GPS AR+LEO AR in east, north and up components is improved from 0.008, 0.008 and 0.027 m to 0.002, 0.003 and 0.011 m, respectively, and the corresponding accuracy within 60 min is improved from 0.002, 0.002 and 0.009 m to 0.001, 0.001 and 0.004 m.

Table 5 Statistical results of hourly static PPP at all 10 stations on March 31, 2019

Type of solution	Frequency of LEO satellites	Convergence time (min)	TTFF (min)	Fixing rate (%)	Positioning accuracy within 10 min (m)			Positioning accuracy within 60 min (m)		
					East	North	Up	East	North	Up
GPS	–	17.9	–	–	0.075	0.092	0.152	0.020	0.010	0.021
GPS+LEO	$f_{L} + f_{S\text{-up}}$	2.5	–	–	0.008	0.008	0.027	0.002	0.002	0.009
GPS+LEO AR		2.5	9.9	58.6	0.006	0.006	0.023	0.001	0.002	0.009
GPS AR+LEO AR		2.4	5.0	100.0	0.002	0.003	0.011	0.001	0.001	0.004
GPS+LEO	$f_{L\text{-up}} + f_{C}$	2.2	–	–	0.008	0.008	0.026	0.002	0.002	0.009
GPS+LEO AR		2.2	55.6	6.4	0.008	0.008	0.026	0.002	0.002	0.009
GPS AR+LEO AR		2.2	4.9	99.2	0.003	0.003	0.011	0.001	0.001	0.005

Conclusions and outlook

We propose a feasible frequency scheme of using the combined frequencies in the L, S and C bands for LEO-based navigation augmentation signals. Compatibility, interoperability and the specific frequency ratio related to dual-band IF PPP AR have been considered in frequency design. In terms of signal modulation, a high-efficiency modulation scheme called CPM is adopted to satisfy the strict out-of-band constraints in the S and C bands. The potential interference from designed signals to the existing navigation systems, RA and MLS is evaluated based on the SSC, PFD and APFD, and the results show that all designed signals can satisfy the regulation of the ITU. We also investigate the signal propagation characteristics in different bands mainly based on the attenuation models of the ITU. The result shows that in the case of similar satellite transmitted power, the received power of all proposed signals will be stronger than that of the GPS L1 signal, particularly for high elevation angle.

Then, the high-rate GPS+LEO observations at 70 reference network stations and 10 user stations distributed in Europe are simulated and used for FCB estimation and PPP tests, respectively. We find that 100.0% of GPS NL residuals agree well within ±0.15 cycles with a STD of 0.008 cycles, 99.7% of LEO L+S dual-band IF residuals are within ±0.15 cycles with a STD of 0.040 cycles, and only 71.7% of LEO L+C dual-band IF residuals are within ±0.15 cycles with a STD of 0.160 cycles. At user stations, the hourly re-initialized static PPP results show that the convergence time of GPS-only can be significantly shortened from 17.9 to within 2.5 min with the augmentation of about 5.44 LEO satellites. In terms of positioning accuracy, AR solution has an obvious advantage. Compared with ambiguity-float GPS+LEO PPP, the positioning accuracy within 10 min of GPS AR+LEO AR in east, north and up components is improved from 0.008, 0.008 and 0.027 m to 0.002, 0.003 and 0.011 m, i.e., an improvement of 75.0, 62.5, and 59.3%, respectively. In addition, the feasibility of LEO dual-band IF PPP AR even without the help of GPS PPP AR has been verified if of course the frequency choice of LEO satisfy the integer multiple.

Due to space limitations, only static PPP AR tests in open sky situations are carried out. A typical application is to quickly obtain the high-precision absolute coordinates of control points or reference stations during field surveying. In fact, AR is also effective in kinematic PPP and significant improvement will also be found. Typical applications are self-driving cars and unmanned aerial vehicles. PPP in more challenging situations like urban and sub-urban areas has more research significance, which can be considered in the future. In addition to the important role in augmenting fast precise positioning, the LEO-based navigation augmentation system can also bring opportunities to other practical applications and scientific research such as integrated precise orbit determination, space weather monitoring, and indoor positioning (Zhang and Ma 2019).

Future research will further discuss the selection of modulation methods. A quadrature multiplexed modulation scheme will be more conducive to improving the performance of the navigation signal as more power can be allocated to the pilot channel than the data channel (Yao et al. 2010). The acquisition and code tracking errors, the multipath error envelopes, the effective C/N0, compatibility and anti-interference ability will also be analyzed. Additionally, the complicated augmentation system, composed of different geometries, frequencies and signals does increase the burden of the receiver to some extent, and further optimization and improvement are needed.

Acknowledgments

The authors warmly thank Prof. Mingquan Lu at Tsinghua University and Dr. Ye Tian at China Academy of Space Technology for their valuable suggestions, proactive support and interest in this work. This study is financially supported by the National Science Fund for Distinguished Young Scholars (No. 41825009), a Wuhan Science and Technology Project (No. 2018010401011270), and the Changjiang Scholars program. In addition, the numerical calculations in this paper have been done on the supercomputing system in the Supercomputing Center of Wuhan University.

Appendix: PSD expressions of CPM signals

The autocorrelation function of a CPM signal can be expressed as

$$\Re(\tau)=\frac{1}{T}\int_0^T \prod_{i=\lceil 1-L\rceil}^{\lfloor \tau/T\rfloor+1}\frac{1}{M}\cdot\frac{\sin\left\{2\pi hM\cdot\left[q(t+\tau-iT)-q(t-iT)\right]\right\}}{\sin\left\{2\pi h\cdot\left[q(t+\tau-iT)-q(t-iT)\right]\right\}}\mathrm{d}t \tag{24}$$

where T is the symbol duration, and τ is the correlation time. L is the pulse length. M is the modulation order indicating that the data are M-ary symbols. h is the modulation index; only if h>1, spectrum splitting can appear, and the larger the index is, the farther the distance between two main lobes, otherwise, the power spectra has only one main lobe. Note that though a longer L and a bigger M can effectively decrease the amplitude of side lobes, sometimes the feature of spectrum splitting may lose even if h>1. $q(t)$ is the phase response function depends on the shape of the corresponding frequency pulse, for a rectangular pulse, we have

$$q(t)=\begin{cases}0, t\leq 0\\ \dfrac{t}{2LT}, 0<t\leq LT\\ \dfrac{1}{2}, t>LT\end{cases} \tag{25}$$

while for a raised-cosine pulse, we have

$$q(t)=\begin{cases}0, t\leq 0\\ \dfrac{t}{2LT}-\dfrac{1}{4\pi}\sin\left(\dfrac{2\pi t}{LT}\right), 0<t\leq LT\\ \dfrac{1}{2}, t>LT\end{cases} \tag{26}$$

where t is the time. Due to the smoother waveform, the raised-cosine pulse contributes to a stronger spectrum roll-off in side lobes than the rectangular one. Then, the PSD of a CPM signal derived from Fourier transformation of $\Re(\tau)$ is written as

$$\begin{aligned}G_{\mathrm{CPM}}(f)=2\Bigg[&\int_0^{(1-s)T}\Re(\tau)\cos(2\pi f\tau)\mathrm{d}\tau\\ &+\frac{1-\psi(jh)\cos(2\pi fT)}{1+\psi^2(jh)-2\psi(jh)\cos(2\pi fT)}\int_{(1-s)T}^{(2-s)T}\Re(\tau)\cos(2\pi f\tau)\mathrm{d}\tau\\ &-\frac{\psi(jh)\sin(2\pi fT)}{1+\psi^2(jh)-2\psi(jh)\cos(2\pi fT)}\int_{(1-s)T}^{(2-s)T}\Re(\tau)\sin(2\pi f\tau)\mathrm{d}\tau\Bigg]\end{aligned} \tag{27}$$

with

$$\psi(jh)=\sin(M\pi h)/[M\sin(\pi h)] \tag{28}$$

$$s = \lfloor 1 - L \rfloor \quad (29)$$

where f is the frequency. The parameters T, M, L, h and $q(t)$ codetermine the spectral characteristics, and the specific configurations for proposed CPM signals are given in Table 6.

Table 6 Specific configurations for proposed CPM signals

Modulation	T	M	L	h	Frequency pulse
BM1REC(2), h=8	$1/(2\times1.023\ \mathrm{MHz})$	2	1	8	Rectangular
BM2RC(1), h=4	$1/(1\times1.023\ \mathrm{MHz})$	2	2	4	Raised-cosine
BM2RC(3), h=1	$1/(3\times1.023\ \mathrm{MHz})$	2	2	1	Raised-cosine

References

Avila-Rodriguez JA, Wallner S, Won JH, Eissfeller B, Schmitz-Peiffer A, Floch JJ, Colzi E, Gerner JL (2008) Study on a Galileo signal and service plan for C-band. In: Proc. ION GNSS 2008, Institute of Navigation, Savannah, GA, USA, September 16–19, 2515–2529

Banville S (2016) GLONASS ionosphere-free ambiguity resolution for precise point positioning. J Geod 90(5):487–496

Dai L (2000) Dual-frequency GPS/GLONASS real-time ambiguity resolution for medium-range kinematic positioning. In: Proc. ION GPS 2000, Institute of Navigation, Salt Lake City, UT, USA, September 19–22, 1071–1080

Ge H, Li B, Ge M, Zang N, Nie L, Shen Y, Schuh H (2018) Initial assessment of precise point positioning with LEO enhanced global navigation satellite systems (LeGNSS). Remote Sens 10(7):984

Guo K, Aquino M, Veettil SV (2019) Ionospheric scintillation intensity fading characteristics and GPS receiver tracking performance at low latitudes. GPS Solut 23(2):43

Hu J, Zhang X, Li P, Ma F, Pan L (2019) Multi-GNSS fractional cycle bias products generation for GNSS ambiguity-fixed PPP at Wuhan University. GPS Solut 24(1):15

Irsigler M, Hein GW, Schmitz-Peiffer A (2004) Use of C-band frequencies for satellite navigation: benefits and drawbacks. GPS Solut 8(3):119–139

IS-GPS-200 (2010) Interface specification: Navstar GPS space segment/navigation user interfaces, IS-GPS-200, Revision E, GPS Wing (GPSW) Systems Engineering and Integration, June 8

Issler JL, Paonni M, Eissfeller B (2010) Toward centimetric positioning thanks to L- and S-band GNSS and to meta-GNSS signals. In: Proceedings of the 5th ESA Workshop on Satellite Navigation Technologies and European Workshop on GNSS Signals and Signal Processing, Toulouse, France, December 8–10, 1–8

ITU-R (2005) Specific attenuation model for rain use in prediction methods. ITU-R Recommendation P.838-3

ITU-R (2009) Attenuation due to clouds and fog. ITU-R Recommendation P.840-4

ITU-R (2013) Attenuation by atmospheric gases. ITU-R Recommendation P.676-10

ITU-R (2015) Propagation data and prediction methods required for the design of earth-space telecommunication systems. ITU-R Recommendation P.618-12

Kouba J (2009) A guide to using International GNSS Service (IGS) products. http://www.acc.igs.org/UsingIGSProductsVer21.pdf

Laurichesse D, Mercier F, Berthias JP, Broca P, Cerri L (2009) Integer ambiguity resolution on undifferenced GPS phase measurements and its application to PPP and satellite precise orbit determination. Navigation 56(2):135–149

Lawrence D, Cobb HS, Gutt G, Connor MO, Reid TGR, Walter T, Whelan D (2017) Innovation: Navigation from LEO. GPS World, June 2017

Li X, Ma F, Li X, Lv H, Bian L, Jiang Z, Zhang X (2019) LEO constellation-augmented multi-GNSS for rapid PPP convergence. J Geod 93(5):749–764

Lu M, Yao Z, Zhang J, Guo F, Wei Z (2015) Progress and development trend of signal design for BeiDou satellite navigation system. Satell Appl (12):27–31 **(in Chinese)**

Ma F, Zhang X, Li X, Cheng J, Guo F, Hu J, Pan L (2020) Hybrid constellation design using a genetic algorithm for a LEO-based navigation augmentation system. GPS Solut 24(2):62

Mateu I, et al. (2009) Exploration of possible GNSS signals in S-band. In: Proc. ION GNSS 2009, Institute of Navigation, Savannah, GA, USA, September 22–25, 1573–1587

Reid TGR, Neish AM, Walter TF, Enge PK (2016) Leveraging commercial broadband LEO constellations for navigation. In: Proc. ION GNSS+ 2016, Institute of Navigation, Portland, OR, USA, September 12–16, 2300–2314

Sun Y, Xue R, Zhao D, Wang D (2017) Radio frequency compatibility evaluation of S band navigation signals for future BeiDou. Sensors 17(5):1039

Teunissen PJG (1995) The least-squares ambiguity decorrelation adjustment: a method for fast GPS integer ambiguity estimation. J Geod 70(1–2):65–82.

Teunissen PJG, Joosten P, Tiberius CCJM (1999) Geometry-free ambiguity success rates in case of partial fixing. In: Proc. ION NTM 1999, Institute of Navigation, San Diego, CA, USA, January 25–27, 201–207

Van Dierendonck AJ, Klobuchar J, Hua Q (1993) Ionospheric scintillation monitoring using commercial single frequency C/A code receivers. In: Proc. ION GPS 1993, Institute of Navigation, Salt Lake City, UT, USA, September 22–24, 1333–1342

Wang L, et al. (2019) Initial assessment of the LEO based navigation signal augmentation system from Luojia-1A satellite. Sensors 18(11):3919

Xie J, Kang C (2021) Engineering innovation and the development of the BDS-3 navigation constellation. Engineering 7(5):558–563

Xue R, Sun Y, Zhao D (2015) CPM signals for satellite navigation in the S and C bands. Sensors 15(6):13184–13200

Yang Y (2016) Concepts of comprehensive PNT and related key technologies. Acta Geod Cartogr Sin 45(5):505–510 (**in Chinese**)

Yao Z, Lu M, Feng Z (2010) Quadrature multiplexed BOC modulation for interoperable GNSS signals. Electron Lett 46(17):1234–1236

Zhang X, Ma F (2019) Review of the development of LEO navigation-augmented GNSS. Acta Geod Cartogr Sin 48(9):1073–1087 (**in Chinese**)

Zhao Q, Li X, Liu Y, Geng J, Liu J (2018) Undifferenced ionospheric-free ambiguity resolution using GLONASS data from inhomogeneous stations. GPS Solut 22(1):26

Author biographies

Fujian Ma is currently an engineer at China Academy of Space Technology. He obtained his Ph.D. degree from Wuhan University in 2021. His current research focuses on the augmentation of multi-GNSS PPP with a LEO constellation.

Xiaohong Zhang is currently a professor at Wuhan University. He obtained his B.Sc., M.Sc. and Ph.D. degrees with distinction in Geodesy and Engineering Surveying from Wuhan University in 1997, 1999, and 2002. His main research interests include PPP, PPP-RTK, GNSS/INS integration technology, and its applications.

Jiahuan Hu is currently a Ph.D. candidate at York University. He obtained his M.Sc. degree from Wuhan University in 2020. His main research interest is multi-GNSS PPP AR.

Pan Li is a research scientist at the German Research Centre for Geosciences (GFZ), Germany. He obtained his Ph.D. degree in 2016 from Wuhan University, China. His current research focuses mainly on GNSS PPP AR.

Lin Pan is currently an associate professor at Central South University. He obtained his Ph.D. degree from Wuhan University in 2018. His current research is mainly focused on GNSS PPP.

Siqi Yu is currently an engineer at Qianxun Spatial Intelligence Inc. She obtained her Ph.D. degree from Wuhan University in 2019. Her current research focuses on GNSS/INS integrity monitoring.

Zhiyu Zhang obtained his M.Sc. degree from Wuhan University in 2020 where he is currently a Ph.D. candidate. His current research focuses on GNSS remote sensing.